Robotic knot tying through a spatial trajectory with a visual servoing system

Bo Lu, Henry K. Chu, and Li Cheng
bo.lu@connect.polyu.hk, henry.chu@polyu.edu.hk, mmlcheng@polyu.edu.hk

***Abstract*— Robot assisted surgery has become increasingly popular with the rapid development of more sophisticated robotic systems. Nevertheless, there are still many tedious surgical tasks that remain to be performed manually by surgeons with high supervisions. One example is to tie a surgical knot during the surgery, which includes the processes of needle threading, suture looping, suture tail grasping and suture pulling. In this research, we present a new method for robotic suture looping process. This method is based on a spatial trajectory planning for the surgical instruments, where challenges such as suture slippage and potential collisions between the instruments could be eliminated. In contrast to conventional looping process, a dynamic control scheme is proposed to optimize the time and workspace required to complete the process. Vision information is incorporated in order to enable closed loop control of the robotic system with Linear Quadratic (LQ) controller. A series of experiments were conducted in order to examine the performance of the proposed control scheme and the results confirmed that surgical knots can be successfully tied robotically, offering new insights to the field of automated robot-assisted surgery.**

I. INTRODUCTION

The research on robot-assisted surgery has been conducted for many years. Tracing back to decades ago, a modified PUMA robot was used to guide a needle in a patient for brain biopsy [1]. With the advancement of robot technology, more than 200,000 surgical procedures were performed yearly through a da Vinci Surgical System, offering new alternatives to traditional open surgery and conventional laparoscopy. While the da Vinci system provides an excellent platform for general surgeries, there remains a high demand on the exploration of more intelligent and robust robotic systems to suit the needs of different surgical procedures.

To date, a number of robotic systems have been reported. For instance, Kapoor et al. [2] developed a hybrid 8 Degrees-of-Freedom (DOFs) experimental robot. This robot adopted a high level control and an optimization framework to assist suturing in a confined space inside the throat. Matsuno et al. [3] proposed a vision-based robotic system with a flexible object recognition method, which can compensate the need of haptic sensory during the surgery. In addition, Martel et al. [4] introduced a video processing method, which can monitor the suture strain during the surgery. This system can successfully detect very small strains, and the use of visual feedback can improve the success rate of robotic surgery.

Surgical robots with vision guideline and sensory feedback have become nowadays standards in robot-assisted surgery. Combining with different control schemes, many tedious surgical tasks could now be performed automatically so that the surgeon workload can be significantly reduced, thereby minimizing the likelihood of human error caused by fatigue.

In this paper, a new robotic system and the employed control algorithm for automated surgical task execution is presented and the outline of the paper is as follows: Section II gives a brief review on the related research. Section III describes the considerations for trajectory planning and tracking through vision images. The control algorithm, based on the transformation matrix calibrated experimentally, for closed-loop control of the system is presented in Section IV. Results from the experiments and the summary are discussed in the two last sections of the paper.

II. RELATED WORK

Suturing is a simple yet tedious and repetitive task during the surgery and tying a surgical knot with a robotic system could be performed in a number of ways. For instance, Chow et al. [5] examined robotic knot tying through vision guidance, where the suture looping was performed by a "roll arc looping" approach. In their following research [6], three more suture looping approaches were proposed in order to optimize the trajectory and workspace required for knot tying. Nevertheless, the suture may not maintain in tension throughout the process due to continuous movements of the grippers. In [7], Osa et al. developed a framework for online trajectory planning that is adaptive to the surrounding dynamic environment. The system was first trained through a demonstration under various states of the environment, and the trajectory under the given environmental conditions is computed using the learned model. The robustness of the system was examined by intentionally disrupting one of the surgical instruments during the task and the trajectory was adapted to the new position. Similar to many learning approaches, the accuracy of this method relies on the training dataset, where dataset from the real surgical scene could be hard to obtain. Nageotte et al. [8] proposed a theoretical approach to complete the stitching task in laparoscopic surgery through kinematic analysis and geometric modeling. By properly choosing the state variables, the possible path that can minimize tissue deformation while driving the needle towards the desired target was computed and simulated. Duan et al. [9] proposed a 3D curvature-constrained trajectory planning using sequential convex optimization. One key advantage of this method is the capability of generating trajectories for multiple instruments that are mutually

collision-free. In [10], Sen et al. developed a suture needle angular positioner (SNAP) algorithm for automated multi-throw suturing. Through a da Vinci system, four-throw task was successfully performed. Nevertheless, occlusions during the experiments could greatly affect the performance on needle pose estimation and needle re-grasping.

Although the aforementioned and many other studies [11-13] have made significant contributions to the field of robotic surgery, there remain many areas that can be further developed. In this research, we aim to provide to a solution towards automated surgical knot tying through an in-house robotic system. This system adopts a configuration with fewer DOFs than the commercial da Vinci surgical system, providing an economic alternative for small-scale surgery. Compared to our previous work, visual information was incorporated in the control algorithm for closed-loop control and the performance of the proposed algorithm was examined experimentally. A two-throw surgical knot was performed to demonstrate the effectiveness of the algorithm.

In contrast to other research that adopts stereovision for 3D positioning of the surgical instruments, this research employed a single vision camera to compute the necessary position information, thereby reducing the computation cost and the complexity on system setup. Pattern matching algorithm was adopted to extract the information from the images, eliminating the need of adding markers on standard surgical instruments.

III. Trajectory for Surgical Knot Tying

A. Vector Representation

The most important part in tying a surgical knot is to wind the suture around the gripper (needle holder) for two or more loops. The spatial trajectories that can prevent suture slippage while winding the suture loops dynamically with two surgical instruments were first presented in [13]. In order to command the two surgical instruments to follow their planned trajectory, visual information was incorporated to enable closed-loop control. In this paper, the vector, $\vec{\mathcal{D}}$, denotes the desired coordinates of the grippers, with respect to the robot origin, through the pre-planned trajectory. The vector, $\vec{\imath}$, denotes the current coordinates of the grippers in the image frame. Through an experimentally obtained transformation matrix $\mathcal{T}$, the correlation between the grippers in the image frame and in the robot frame can be determined to calculate the robot coordinates of grippers, represented as $\vec{\mathcal{R}}$, accordingly. The errors between the current position and the desired position of each gripper is used to compute the vector, $\vec{\mathcal{M}}_s$, which send to the system for moving the grippers.

B. Visual-based Trajectory Tracking and Control

The process of suture winding through trajectory tracking and control can be summarized in the following steps: Prior to the experiment, a high-resolution CMOS camera on a stand was adjusted to provide an optimal view for the current surgical situation. An RGB image showing the current manipulating area (background) was captured and two surgical instruments were guided to manipulate towards the two suture ends to complete the initial setup. Then, real-time images captured from the camera were transferred to a computer for image processing. A custom C++ program was used to extract relevant visual information for control purpose. Since the influence from the ambient environment, such as light intensity and background noise, could affect the quality of the images, Gaussian Blur was employed to filter and smoothen the real-time images. Then, background subtraction algorithm was implemented to enhance the image for evaluating the moving objects of interest. As shown in Figure 1, the RGB matrices of a real-time image were subtracted by the background image, resulting a nearly black image for the detection of the two grippers.

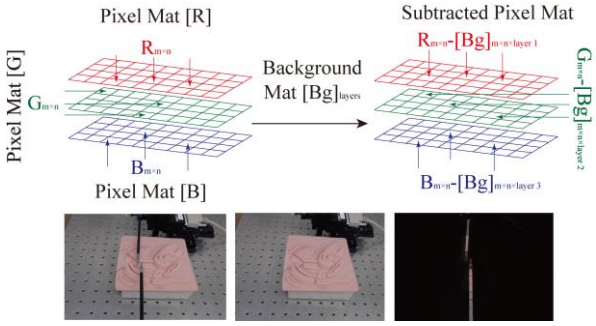

Figure 1. Subtraction of Real-time Images using the Background

Next, the two grippers in the images were identified using the Pattern Matching algorithm. In our research, we chose $SQDIFF\_NORMED$ approach to search for the corresponding locations of two grippers. Figure 2 shows the images from the camera at two instances, after performing background subtraction and Gaussian filtering. Using the Pattern Matching algorithm, these two grippers were successfully detected and displayed on the screen.

$$SQDIFF\_NORMED_{(x,y)} = \frac{\sum_{x',y'}(T(x',y')-I(x+x',y+y'))^2}{\sqrt{\sum_{x',y'}T(x',y')^2 \cdot \sum_{x',y'}I(x+x',y+y')^2}} \quad (1)$$

where (x, y) denotes the current coordinates being examined, I and T denote the source and template images, respectively.

Figure 2. Identifications of Grippers in Camera's Frame

Image coordinates of the two grippers were evaluated and fed to the C++ program. Then, transformation between the image coordinates and the robot coordinates was performed through a transformation matrix. Finally, the desired trajectories for the two grippers that can complete the knot tying process were discretized into multiple segments, and the errors between the current and desired coordinates of the grippers were calculated. The control inputs for the system were then consequently figured out. In contrast to other work

[3, 5], this selected method does not require integrating distinctive features onto the tools nor using multiple cameras for tracking, providing a simpler hardware setup for use in surgery.

During the experiment, information such as the current positions of two grippers and the control inputs can be displayed through the program and users can monitor the process in real-time and terminate in case of any abnormal operations.

IV. METHOD

A. Transformation Matrix

As discussed, the gripper coordinates in the image plane, $\vec{\imath}$, and their respective coordinates in the robot frame, $\vec{\mathcal{R}}$, can be related with a transformation matrix $\mathcal{T}$, using the equation:

$$\vec{\mathcal{R}} = \mathcal{T} \cdot \vec{\imath} \tag{2}$$

For a fully calibrated vision system, the transformation matrix can be evaluated using the intrinsic and extrinsic camera parameters. Alternatively, the transformation matrix can also be obtained through experiments [14, 15]. The vision system in this research is configured based on the following two considerations:

(1). The workspace required to complete the operation is approximately 30mm × 30mm × 30mm (as shown in Figure 5). Hence, the field of view of the vision system must be sufficient to capture the entire process after initial setup and remains stationary throughout the process.

(2). The robotic system is capable of providing three degrees of motions (X, Y, Z) to the grippers. To perform suture winding, the grippers are manipulated following their planned trajectories, which lie in the Y-Z plane. The positions of the grippers in the X-axis remain stationary. As a result, the captured image from the vision system must be able to extract relative change in the position information in the Y-Z plane.

Figure 3 illustrates the schematic diagram of the experimental setup. In order to minimize possible occlusions, the camera is tilted at an angle when viewing the two grippers from the side view, as shown in Figure 3. As the grippers displace from their original positions, shown in light color, the grippers at the new positions remain lies in the Y-Z plane, as shown in dark color.

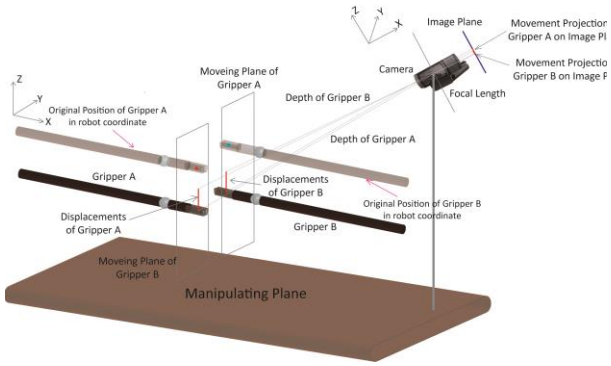

Figure 3. Sketch of the Manipulating Space

Before evaluating $\mathcal{T}$, one assumption has to be made. The transformation matrix is known to be dependent on parameters such as the depth of the object with respect to the camera and the magnification factors. As shown in Figure 3, the moving plane and the image plane of the system are not in parallel. Also, the initial positions of the two grippers may not necessarily align with the optical axis (the center of the image). Their origin offsets can be corrected through translation vectors. When the two grippers move in the Y-Z plane, the depth distance between the grippers and the camera changes as well. Nevertheless, such change is relatively small as compared to the initial depth (over 300mm). Hence, the influence on the transformation matrix becomes negligible and the matrix can be approximated to be constant throughout the operation, and iterative update on the matrix estimation is not necessary [16].

The method to estimate $\mathcal{T}$ is based on the approach described in [14]. Point features were moved to different robot coordinates and their corresponding changes in the image coordinates were extracted from the images and used to construct two matrices. In contrast to the work in [14], the origins of the two coordinate planes were not aligned and translation vectors [17] were added during the computation to account for the origin offset.

With reference to the system setup in Figure 3, images of the two grippers projected on the image plane are shown in Figure 4. Let the position vectors of the grippers with respect to the image coordinates ($\vec{\imath}_n$) and the robotic coordinates ($\vec{\mathcal{R}}_n$) be:

$$\vec{\imath}_n = \begin{Bmatrix} \mathrm{x}_i^n \\ \mathrm{y}_i^n \\ \mathrm{z}_i^n \end{Bmatrix} \quad \vec{\mathcal{R}}_n = \begin{Bmatrix} \mathrm{x}_{\mathcal{R}}^n \\ \mathrm{y}_{\mathcal{R}}^n \\ \mathrm{z}_{\mathcal{R}}^n \end{Bmatrix} \tag{3}$$

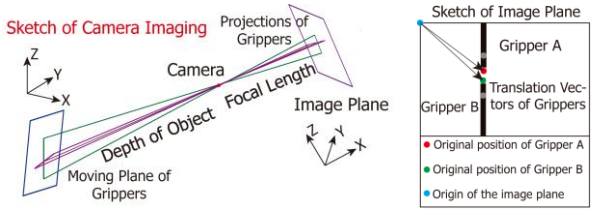

Figure 4. Sketches of Camera Imaging and Image Plane

where n denotes the label of gripper, "A" or "B".

The number of movements of the point features used in evaluating the transformation matrix is important towards the convergence of the matrix. To balance between accuracy and computation cost, a total of 11 movements in the Y-Z plane were considered. The transformation matrix that can map between the image coordinates and the robot coordinates can be computed as:

$$\mathcal{T}_n = (\mathcal{T}_{\mathcal{R}})_n \cdot (\mathcal{T}_i^{\mathrm{T}})_n \cdot \left[(\mathcal{T}_i)_n \cdot (\mathcal{T}_i^{\mathrm{T}})_n\right]^{-1} \tag{4}$$

where $\mathcal{T}_n$ denotes the transformation matrix of Gripper n, $(\mathcal{T}_{\mathcal{R}})_n$ and $(\mathcal{T}_i)_n$ are the matrices that can be obtained through experimental data. Their expressions are given in equation (5), where $[(\mathrm{y}_{\mathcal{R}}^n)_{\mathrm{N}}, (\mathrm{z}_{\mathcal{R}}^n)_{\mathrm{N}}]$ are robot coordinates of

Gripper n at the Nth movement in the Y-Z plane, and $[(y_i^n)_N, (z_i^n)_N]$ are the corresponding image coordinates of Gripper n at the Nth movement.

B. Optimal Control Scheme

The desired trajectories are generated aiming to eliminate the potential risks of suture's slippage and to save the required workspace, as described in [13]. Following the trajectories, the two grippers can be guided to complete the specified operation. Figure 5 illustrates the desired coordinates of the two grippers along the trajectories, where bigger circles indicate the important intermediate points in the trajectories. Compared with the looping method proposed in [5, 6], the required work space in our research can be reduced up to 40%. The inputs of the manipulators were determined by discretizing the trajectories into multiple segments. To enhance the precision in manipulating the grippers to follow their respective trajectory, vision feedback was adopted for closed-loop control purpose.

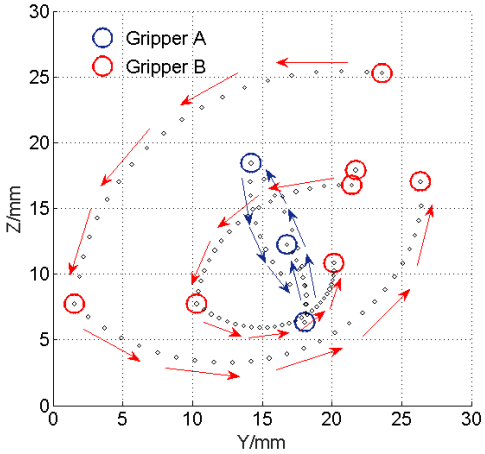

Figure 5. Subsections of Grippers' Trajectories

Using the transformation matrix and the visual information, the positions of the two grippers with respect to the robot coordinates in kth step can be figured out as:

$$\vec{\mathcal{R}}_n(k) = \mathcal{T}_n \cdot \left[\vec{\imath}_n(\mathrm{k}) - \vec{\imath}_{BORG}^{\,n}\right] \tag{6}$$

where $\vec{\mathcal{R}}_n(\mathrm{k})$ is the vector denoting the robot coordinates of the gripper in kth step, $\vec{\imath}_{BORG}^{\,n}$ is the translation vector of the gripper with respect to the image origin.

In order to account for uncertainty or disturbances during the experiment, a controller was added to the robotic system to provide tunability on the performance of the gripper movements. The controller was designed using the Linear Quadratic (LQ) control scheme because of its advantage on the implementation. Vision-based control with this LQ controller have been employed for applications in microscale manipulation [18, 19], but their focuses are mainly on guiding the target to a desired, fixed positions. In this research, the LQ controller was implemented to track the planned trajectories and the state-equation of the robotic system can be expressed as:

$$\vec{\mathcal{R}}_n(\mathrm{k}+1) = \mathcal{A} \cdot \vec{\mathcal{R}}_n(\mathrm{k}) + \mathcal{B} \cdot \vec{u}_n(\mathrm{k}) \tag{7}$$

where $\vec{\mathcal{R}}_n(\mathrm{k}+1)$ is the vector that denotes the robot coordinates of the gripper in the $(k+1)$th step, $\vec{u}_n$ is the optimal control input, A and B are the system matrices, $\mathcal{A} \in \Re^{2\times2}$, $\mathcal{B} \in \Re^{2\times2}$.

The control objective of the LQ controller is based on the minimization of an objective function that places a cost on errors in the robot coordinates between the current and the desired positions of the grippers, $[\vec{\mathcal{R}}_n(\mathrm{k}+1) - \vec{\mathcal{D}}_n(\mathrm{k}+1)]$, and a cost on the control input, $\vec{u}_n(\mathrm{k})$, where they can be expressed as:

$$\mathrm{E}(\mathrm{k}+1) = \left[\vec{\mathcal{R}}_n(\mathrm{k}+1) - \vec{\mathcal{D}}_n(\mathrm{k}+1)\right]^{\mathrm{T}} \cdot \mathrm{Q} \cdot \left[\vec{\mathcal{R}}_n(\mathrm{k}+1) - \vec{\mathcal{D}}_n(\mathrm{k}+1)\right] - \vec{u}_n{}^{\mathrm{T}}(\mathrm{k}) \cdot \mathcal{L} \cdot \vec{u}_n(\mathrm{k}) \tag{8}$$

where $\mathcal{Q}$ and $\mathcal{L}$ are weighting matrices, $(\mathcal{Q}\ \&\ \mathcal{L}) \in \Re^{2\times2}$.

Taking derivatives of the above equation, the optimal control input $\vec{u}_n(\mathrm{k})$ can be further derived as:

$$\vec{u}_n(\mathrm{k}) = -[\mathcal{B}^{\mathrm{T}}\mathcal{Q}\mathcal{B} + \mathcal{L}]^{-1}\mathcal{B}^{\mathrm{T}}\,\mathcal{Q}[\vec{\mathcal{R}}_n(\mathrm{k}) - \vec{\mathcal{D}}_n(\mathrm{k}+1)] \tag{9}$$

The two weighting matrices, $\mathcal{Q}$ and $\mathcal{L}$, can provide tunability on the system performance by setting more or less emphasis on the error of the gripper positions, and on the

---

Equation (5): (note: $\vec{\imath}_{BORG}^{\,n} = [y_i^{n^*}, z_i^{n^*}]$)

$$(\mathcal{T}_{\mathcal{R}})_n = \begin{bmatrix} (y_{\mathcal{R}}^n)_1 - \frac{1}{\mathrm{N}}\sum_{\mathrm{j}=1}^{\mathrm{N}}(y_{\mathcal{R}}^n)_{\mathrm{j}} & (y_{\mathcal{R}}^n)_2 - \frac{1}{\mathrm{N}}\sum_{\mathrm{j}=1}^{\mathrm{N}}(y_{\mathcal{R}}^n)_{\mathrm{j}} & \dots & (y_{\mathcal{R}}^n)_{\mathrm{N}} - \frac{1}{\mathrm{N}}\sum_{\mathrm{j}=1}^{\mathrm{N}}(y_{\mathcal{R}}^n)_{\mathrm{j}} \\ (z_{\mathcal{R}}^n)_1 - \frac{1}{\mathrm{N}}\sum_{\mathrm{j}=1}^{\mathrm{N}}(z_{\mathcal{R}}^n)_{\mathrm{j}} & (z_{\mathcal{R}}^n)_2 - \frac{1}{\mathrm{N}}\sum_{\mathrm{j}=1}^{\mathrm{N}}(z_{\mathcal{R}}^n)_{\mathrm{j}} & \dots & (z_{\mathcal{R}}^n)_{\mathrm{N}} - \frac{1}{\mathrm{N}}\sum_{\mathrm{j}=1}^{\mathrm{N}}(z_{\mathcal{R}}^n)_{\mathrm{j}} \end{bmatrix}$$

$$(\mathcal{T}_i)_n = \begin{bmatrix} ((y_i^n)_1 - y_i^{n^*}) - \frac{1}{\mathrm{n}}\sum_{\mathrm{j}=1}^{\mathrm{n}}((y_i^n)_{\mathrm{j}} - y_i^{n^*}) & \dots & ((y_i^n)_{\mathrm{N}} - y_i^{n^*}) - \frac{1}{\mathrm{N}}\sum_{\mathrm{j}=1}^{\mathrm{N}}((y_i^n)_{\mathrm{j}} - y_i^{n^*}) \\ ((z_i^n)_1 - z_i^{n^*}) - \frac{1}{\mathrm{N}}\sum_{\mathrm{j}=1}^{\mathrm{N}}((z_i^n)_{\mathrm{j}} - z_i^{n^*}) & \dots & ((z_i^n)_{\mathrm{N}} - z_i^{n^*}) - \frac{1}{\mathrm{N}}\sum_{\mathrm{j}=1}^{\mathrm{N}}((z_i^n)_{\mathrm{j}} - z_i^{n^*}) \end{bmatrix}$$

control input, respectively. In this research, the two matrices were chosen to be diagonal matrices with the expression:

$$\mathcal{Q} = t_1 \cdot I$$

$$\mathcal{L} = t_2 \cdot I \tag{10}$$

where I is an identity matrix, t_1 and t_2 are the tuning parameters of $\mathcal{Q}$ and $\mathcal{L}$.

The optimal values for t_1 and t_2 can be evaluated through experiments and when the system is at optimal, the error between the current and the desired coordinates can be gradually bounded to a stable, minimal value.

In this research, the grippers attached to the robotic system can move independently on each of the three axes. Therefore, the system matrices $\mathcal{A}$ and $\mathcal{B}$ related to the motions in the Y-Z planes can be simplified as:

$$\mathcal{A} = \mathcal{B} = \begin{bmatrix} 1 & 0 \\ 0 & 1 \end{bmatrix} \tag{11}$$

Since the robotic system is commanded in terms of global robot coordinates, the computed relative movements through the LQ method in each step are transformed back to the global frame through the Eq. (12):

$$\left(\vec{\mathcal{M}}_s\right)_n(\mathrm{k}) = \vec{\mathcal{R}}_n(\mathrm{k}) + \vec{u}_n(\mathrm{k}) - \vec{S}_n \tag{12}$$

where the vector $(\vec{\mathcal{M}}_s)_n$ is the command sent to the robotic system for Gripper n, and, $\vec{S}_n = (y_0^n, z_0^n)$ is the offset vector between the origins of the frames.

Due to the influence from the environment, the gripper position measured from the images at different intervals (steps) could be fluctuating even if the gripper has already reached the desired position. To minimize unnecessary command, a threshold $\overrightarrow{\mathcal{TS}}$ is adopted for checking. If the control input is less than a preset threshold value, the gripper will remain at the same position as in the previous step.

Using the above control strategy, the two grippers can be visually guided and follow the planned trajectories in order to complete the surgical knot tying operation. Figure 6 summarizes the main working loop:

(1) Identify the current image coordinates of the gripper $\vec{\imath}_n(\mathrm{k})$;

(2) Employ the transformation matrix $\mathcal{T}_n$ to convert to the Cartesian coordinates of grippers $\overrightarrow{\mathcal{R}_n}(\mathrm{k})$ in robotic system;

(3) Compare between the desired and the current coordinates to obtain $\vec{u}_n(\mathrm{k})$;

(4) Follow the LQ control scheme and compute the control input for next step $(\overrightarrow{\mathcal{MS}})_n(\mathrm{k})$.

V. Experiments and Results

The robotic system used to conduct the experiment is shown in Figure 7. Two standard laparoscopic graspers are attached to two MP-285 manipulators that can provide 3 DOFs, and these manipulators are connected to the MPC-200 controller. A high-resolution camera is used for monitoring and the knot tying is performed on an artificial tissue. The entire system is configured on an anti-vibration table to isolate the noise from the surrounding. A series of experiments were conducted to examine the performance of the proposed control strategy.

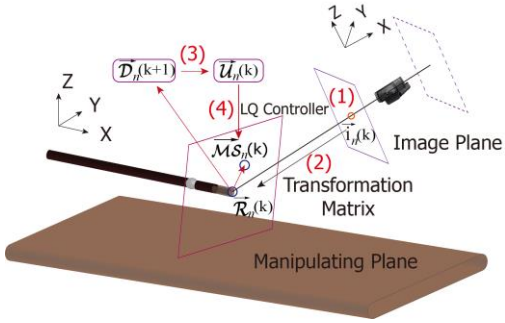

Figure 6. Transformation between the Two Coordinates

(a). Validation Experiment

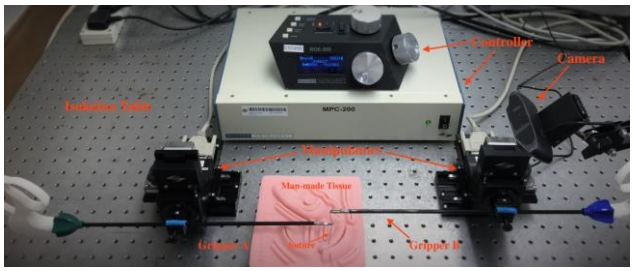

Figure 7. Experimental Setup

In the first experiment, the gripper was commanded to follow a standard, circular trajectory with the proposed control scheme and the tracking performance were evaluated. The radius is set to $5000\,\mu\mathrm{m}$ and the initial position of the trajectory is at $(0,5000)$. The gripper trajectory, in the counter-clockwise direction as shown in Fig. 8(in red) was discretized into 37 segments. The errors between the desired and real positions of the gripper at different intervals can be used to justify whether the transformation matrix and the tuning parameters in LQ control method were appropriate. The circular trajectory can be expressed using the equation:

$$\sqrt{(\mathrm{x_r} - \mathrm{ra})^2 + (\mathrm{y_r} - \mathrm{ra})^2} = \mathrm{ra} \tag{13}$$

where $(\mathrm{x_r}, \mathrm{y_r})$ denotes the robot coordinates along the trajectory, ra is the radius of the circle.

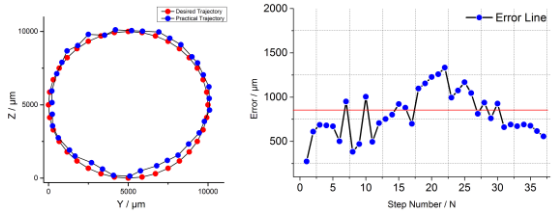

Figure 8. Results of Validation Experiment

Following the procedures described in IV, the manipulator input $(\vec{\mathcal{M}}_s)_n(\mathrm{k})$ was computed and the positions of the

Figure 9. Snapshots of Suture's Looping in Experiment

gripper obtained from the experiment were plotted in Figure 8. From the figure, it is clear that the gripper can follow the trajectory to complete one circular movement. The desired trajectory and the actual trajectory are almost overlapped with each other. The average position error is approximately 750 μm, demonstrating a good tracking performance. Four trials were conducted and similar results (not shown) were obtained, showing good repeatability of the control scheme.

The accuracy of the pattern matching algorithm in evaluating the gripper position was also examined. The gripper was displaced to a new position and image coordinates of the gripper evaluated within 1 minute were recorded. From the collected data, the fluctuation in the coordinates due to noise is within 1 pixel.

(b). Experiment of Surgical Looping

The second experiment is to utilize two grippers to perform the knot tying. An artificial tissue was placed at the center of the image plane and a suture is threaded through the tissue. Based on the results from (a), the trajectories of the two grippers for constructing the first loop were discretized into 68 segments, and each gripper was constrained to move less than approximately 5^{o} of the trajectory arc in each segment. The camera was used to provide visual feedbacks.

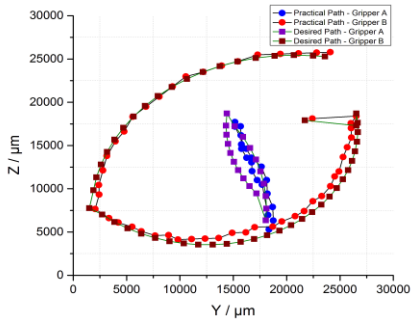

(a). Desired Trajectories and Practical Paths of Two Grippers

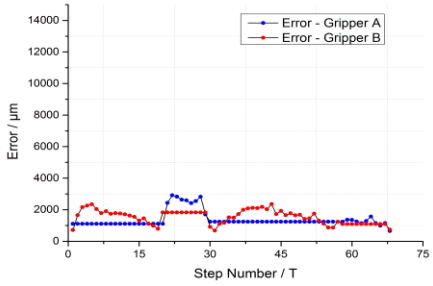

(b). Error of Grippers in Step Domain

Figure 10. Results of Looping Using Two Grippers

Figure 9 shows the snapshots from the experiment at six different intervals. In our experiment, each intersection may take 6 seconds. Following the trajectory, the first loop of a surgical knot can be successfully formed and winded around one gripper. The suture between two grippers and the section between the gripper and the suture's exit point were kept in tension, which can minimize the possibility of suture's slippage. Similar to the first experiment, the trajectories of two grippers and grippers' errors were plotted in Figure 10. From the results, the tracking error was found to increase to 2000μm when performing the suture looping. The reason is mainly due to the bending on the long laparoscopic grippers under the suture tension force.

Without the suture, the tracking error was reduced to less than 1000μm. The experiments were repeated for six times and the suture loops were successfully winded in each of the trial. On average, the tracking error was evaluated to be 1433±45μm.

(c). Experiment of Surgical Looping with Disturbance

To examine the robustness of the algorithm, disturbances were added at three selected locations along the trajectory for gripper B and the gripper was forced to move extra 4000μm away from its position, as shown in Figure 11. From the results, it was found that the tracking error due to the disturbance gradually converged and constrained within the value found in (b), and the gripper followed the pre-planned trajectory to complete the surgical looping.

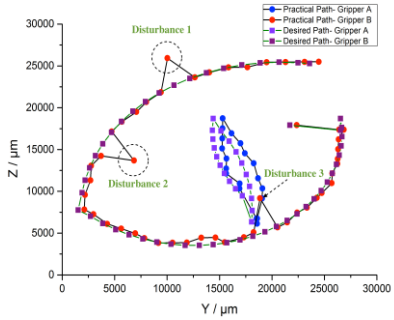

(a). Desired Trajectories and Practical Paths of Two Grippers

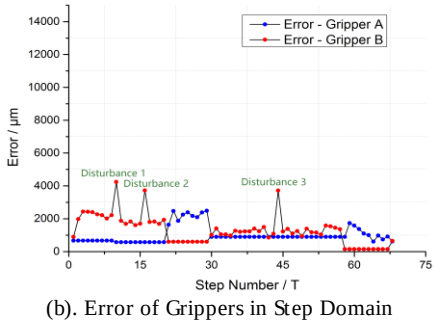

(b). Error of Grippers in Step Domain

Figure 11. Results of Looping Using Two Grippers with Disturbances

VI. CONCLUSION

This paper presents a new method to tie a surgical knot using a robotic system. This system employed two grippers that can move independently to complete the knotting

operation by following planned trajectories. Since the two grippers are manipulated dynamically, the time and workspace required to construct the suture loops can be significantly reduced up to 40% compared with the previous approaches. In order to enhance the accuracy, visual images were incorporated for closed-loop tracking and control of the system. The transformation matrix that can provide mapping between the image coordinates and the robot coordinates was obtained experimentally prior to robotic manipulations, and the LQ control method was adopted to design the controller for the manipulator inputs. Experiments were conducted to show the proposed control scheme can be implemented to move the gripper to follow a circular path. The control scheme was further examined to perform suture looping and experiments were successfully conducted. Based on the findings, the proposed system and the control scheme has the potential to offer a simple and alternative approach for automated robot-assisted surgery.

In the future, the dexterity of the robotic system can be enhanced. Stereo vision can be used to reconstruct the environment of the manipulating conditions with the purpose of extracting more real-time information for precise manipulation and obstacle avoidance.

REFERENCES

1. A. R. Lanfranco, A.E. Castellanos, J. P. Desai, and W. C. Meyers, "Robotic Surgery: A Current Perspective," *Annals of Surgery*, 2004, 239(1), pp. 14–21.
2. A. Kapoor, N.Simaan, and R.H. Taylor, "Suturing in Confined Spaces-Constrained Motion Control of a Hybrid 8-DoF Robot," *Proc. of the 2005 IEEE Int. Conf. on Advanced Robotics*, pp. 452-459.
3. T. Matsuno, T. Fukuda., F. Arai, "Flexible Rope Manipulation by Dual Manipulator System Using Vision Sensor," *Proc. of the 2001 IEEE/ASME Int. Conf. on Advanced Intelligent Mechatronics*, pp. 677-682.
4. J. Martell, T. Elmer, N. Gopalsami, and Y. S. Park, "Visual measurement of suture strain for robotic surgery," *Comp. and Math. Methods in Medicine*, 2011, pp. 1-9.
5. D. Chow, and W. Newman, "Improved Knot-Tying Methds for Autonomous Robot Surgery," *Proc. of the 2013 IEEE Int. Conf. on Automation Science and Engineering*, pp. 461-465.
6. D. Chow and W. Newman, "Trajectory Optimization of Robotic Suturing," *Proc. of the 2015 IEEE Int. Conf. for Practical Robot Applications*, pp. 1-6.
7. T. Osa, N. Sugita, and M. Mamoru, "Online Trajectory Planning in Dynamic Environment for Surgical Task Automation," *Robotics: Science and Systems*, 2014, pp. 1-9.
8. F. Nageotte, P. Zanne, M. de Mathelin, and C. Doignon, "A Circular Needle Path Planning Method for Suturing in Laparoscopic Surgery," *Proc. of the 2005 IEEE Int. Conf. on Robotics and Automation*, pp. 514-519.
9. Y. Duan, S. Patil, J. Schulman, K. Goldberg, and P. Abbeel, "Planning Locally Optimal, Curvature Constrained Trajectories in 3D using Sequential Convex Optimization," *Proc. of the 2014 IEEE Int. Conf. on Robotics and Automation*, 5889-5895.
10. S. Sen, A. Garg, D. V. Gealy, S. McKinley, Y. Jen, and K. Goldberg, "Autonomous Multiple-Throw Multilateral Surgical Suturing with a Mechanical Needle Guide and Optimization based Needle Planning," *Proc. of the 2016 IEEE Int. Conf. on Robotics and Automation*, pp. 4178-4185.
11. H. Kang, and J. T. Wen, "EndoBot: a Robotic Assistant in Minimally Invasive Surgeries," *Proc. of the 2001 IEEE Int. Conf. on Robotics and Automation*, pp. 2031-2036.
12. W. Wang, and D. Balkcom, "Towards arranging and tightening knots and unknots with fixtures," *IEEE Transactions on Automation Science and Engineering*, 2015, 12(4), pp. 1318-1331.
13. B. Lu, H. K. Chu, and L. Cheng, "Dynamic Trajectory Planning for Robotic Knot Tying," *Proc. of the 2016 IEEE Int. Conf. on Real-time Computing and Robotics*, pp. 180-185.
14. L.Wang, L. Ren, J. K. Mills, and W. L. Cleghorn, "Automated 3-D Micrograsping Tasks Performed by Vision-Based Control," *IEEE Tran. on Automation Science and Engineering*, 2010, 7(3), pp. 417-426.
15. H. K Chu, J. K. Mills and W. L. Cleghorn, "Image-based Visual Servoing Through Micropart Reflection For the Microassembly Process," *Journal of Micromechanics and Microengineering*, 2011, 21(6), 065016.
16. J. M. Sebastián, L. Pari, C. González, and L. Ángel, "A New Method for the Estimation of the Image Jacobian for the Control of an Uncalibrated Joint System," *Pattern Recognition and Image Analysis*, 2005, pp. 631-638.
17. M. Dhome, M. Richetin, J. Lapreste, and G. Rives, "Determination of the Attitude of 3-D Objects from a Single Perspective View," *IEEE Tran. On Pattern Analysis and Mach. Intel.*, 1989. 11(12), pp. 1265 - 1278.
18. Y. Sun, and B. J. Nelson, "Biological Cell Injection Using an Autonomous MicroRobotic System," *The Int. Journal of Robotics Research*, 2002, 21:10-11, pp. 861-868.
19. H. Bilen, M. Hocaoglu, E. Ozgur, M. Unel, and A. Sabanovic, "A Comparative Study of Conventional Visual Servoing Schemes in Microsystem Applications," *Proc. of the 2007 IEEE/RSJ Int. Conf. on Intelligent Robots and Systems*, pp. 1308-1313.